

Article

Hydrocarbon Accumulation Analysis Based on Quasi-3D Seismic Data in the Turbulent Area of the Northern South China Sea

Zhongquan Zhao ^{1,2,*}, Guangjian Zhong ¹, Ming Sun ^{1,3,*}, Changmao Feng ³, Guanghong Tu ^{3,*} and Hai Yi ²

¹ Key Laboratory of Marine Mineral Resources, Ministry of Natural Resources, Guangzhou Marine Geological Survey, China Geological Survey, Guangzhou 510075, China

² Southern Marine Science and Engineering Guangdong Laboratory (Guangzhou), Guangzhou 511458, China

³ National Engineering Research Center for Gas Hydrate Exploration and Development, Guangzhou 511457, China

* Correspondence: zzqhello@163.com (Z.Z.); danyifeixiang@126.com (M.S.); tguanghong@mail.cgs.gov.cn (G.T.)

Abstract: The Mesozoic strata in the northern South China Sea have good potential for oil and gas exploration. The Dongsha Waters, where the study area is located, have complex seismic and geological characteristics; in particular, turbulence is very prominent in this area, so it is difficult to implement 3D seismic data collection. The “single-source and single-cable quasi-3D seismic survey” method integrates some key technologies in acquisition and processing, thus improving the quality of seismic imaging. Based on the interpretation of the existing research results and new data, structure B-1 has good source–reservoir–cap combination conditions. The oil–gas accumulation mode is predicted, and the drilling well B-1-1 is given. In addition, the large-scale distribution of bottom-simulating reflectors (BSRs) and the discovery of gas seepage areas in the study area suggest the presence of gas hydrate. We suggest that deep thermogenic gas from the Mesozoic strata has migrated into the overlying strata along the fault system and mixed with microbial gas to form hydrate.

Keywords: quasi-3D seismic; mesozoic; reservoir-forming model; hydrate



Citation: Zhao, Z.; Zhong, G.; Sun, M.; Feng, C.; Tu, G.; Yi, H.

Hydrocarbon Accumulation Analysis Based on Quasi-3D Seismic Data in the Turbulent Area of the Northern South China Sea. *J. Mar. Sci. Eng.* **2023**, *11*, 338. <https://doi.org/10.3390/jmse11020338>

Academic Editor: Timothy S. Collett

Received: 7 December 2022

Revised: 21 January 2023

Accepted: 22 January 2023

Published: 3 February 2023



Copyright: © 2023 by the authors. Licensee MDPI, Basel, Switzerland. This article is an open access article distributed under the terms and conditions of the Creative Commons Attribution (CC BY) license (<https://creativecommons.org/licenses/by/4.0/>).

1. Introduction

As one of the most important stratigraphic intervals for oil and gas exploration, Mesozoic reservoirs contain a huge amount of oil and gas, among which oil accounts for 80.4% and natural gas accounts for 62.9% of the global total, ranking first among all of the oil and gas exploration layers in the world [1–3]. The northern South China Sea (SCS) is the fourth largest oil- and gas-producing area in China [4]. Comprehensive studies show that the Mesozoic strata in the northern SCS have good oil and gas exploration prospects [5–8].

Through years of oil and gas resource investigation and research, the consensus is that the Mesozoic strata are widely developed in the northern part of the SCS [2–4,6–9], among which the Chaoshan depression, which is located in the Dongsha uplift, has the widest distribution area and the largest sedimentary thickness (of over 6000 m) (Figure 1). The Dongsha area in the northern SCS is located at the intersection of the coastal current of the Taiwan Strait and the Kuroshio Current of the Bashi Strait. It has complex seismic geological conditions, which are mainly reflected in the following [3,10,11]: (1) The water depth in the study area varies greatly, and the rugged seabed easily causes seismic wave scattering and energy attenuation; (2) the seabed in some areas is hard (sandstone and carbonate rock), which causes ringing; (3) the deep target strata, complex geological structure and serious multiple waves in the Mesozoic exploration result in a low signal-to-noise ratio in the deep layer; (4) the seismic wave energy decays rapidly due to the shielding effect of shallow carbonate and volcanic rocks and the strong impedance interface formed at the bottom of

the Cenozoic. (5) The formation velocity changed little in the Mesozoic era, and the wave impedance difference between the strata is small, resulting in a weak internal reflection energy. (6) The shallow currents in the Dongsha Waters are rapid, variable in direction and difficult to predict, which is called “turbulence”. This makes it is easy for cable tail sinking damage to occur and the feathering angles to exceed the standards during construction [9] (Figure 2), thus affecting the quality of the field seismic data collection.

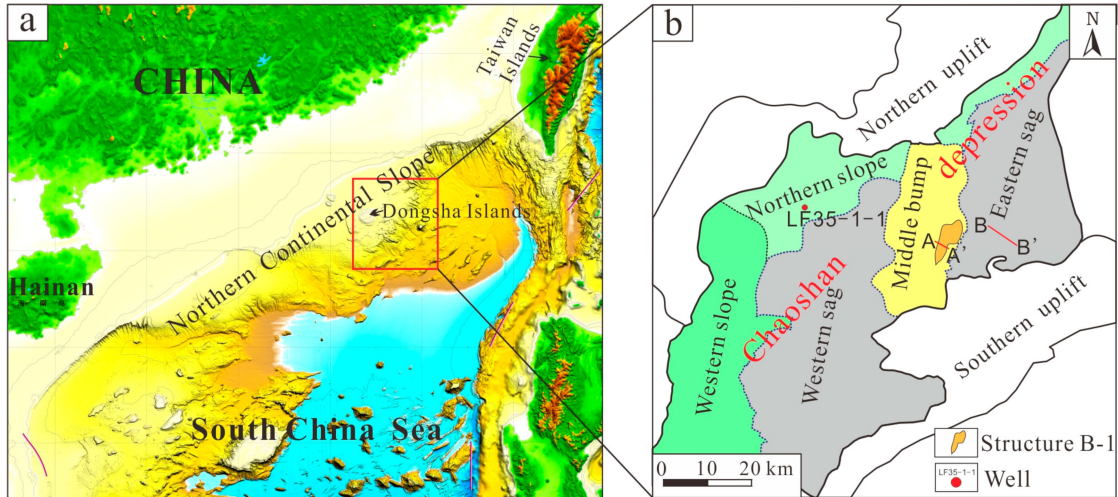


Figure 1. Location and Mesozoic tectonic division of the study area ((a). location of the study area; (b). Mesozoic tectonic division of Chaoshan depression).

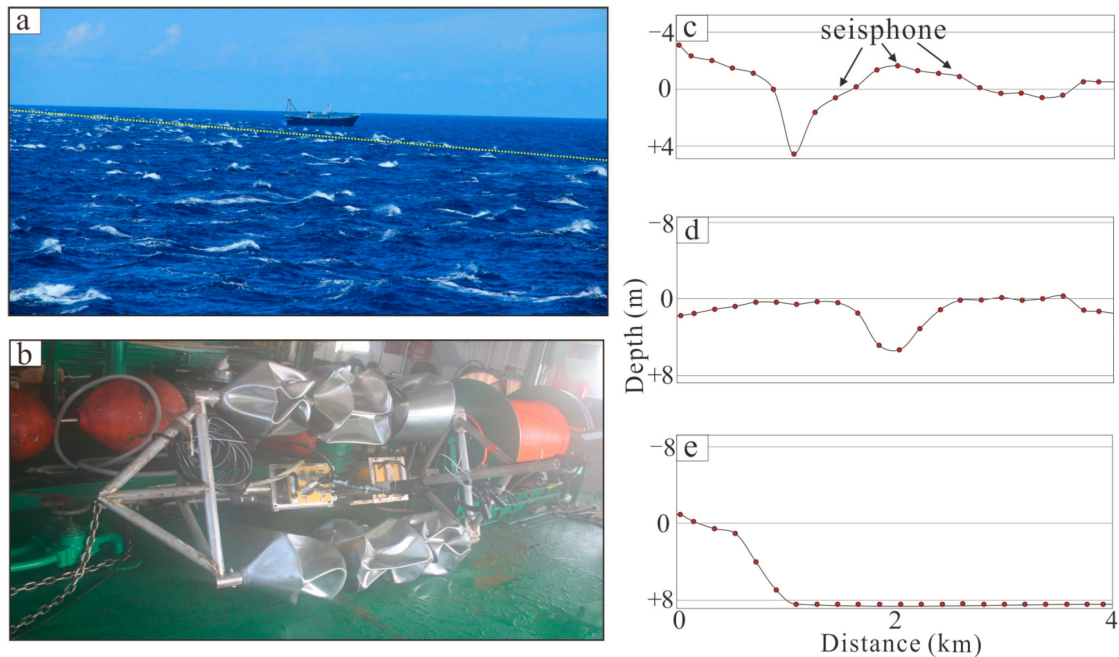


Figure 2. (a) Turbulence zones observed on the sea surface; (b) cable tails damaged by turbulence in deep water; (c–e) turbulence flow influences the location of the seismophones (in general, without the influence of extreme sea conditions, each seismophone should present an approximate horizontal line, with a fluctuation of no more than 1 m).

To expand the exploration areas, improve the situation of Mesozoic oil and gas exploration in the northern area of the SCS and achieve a breakthrough in oil and gas exploration, the China Geological Survey (CGS) has deployed more than 10,000 km of 2D seismic lines in the Chaoshan depression of the Dongsha Waters in the northern part of the SCS in the

past decade. Based on comprehensive seismic and geological research, the Chaoshan depression is further divided into five secondary structural units [3,9,11] (Figure 1b), namely, the eastern sag, the western sag, the middle bump, the northern slope and the western slope. A number of key structures have been delineated, and a series of experiments have been carried out on acquisition and processing techniques for favorable structures.

Due to the special seismic and geological conditions of the Mesozoic strata in the northern SCS, it is difficult for conventional 2D seismic survey methods to obtain high-quality seismic data [12], which does not meet the requirements of oil and gas exploration in mid-deep strata. As the specific time, place, intensity and frequency of the turbulence in the sea area of the study area cannot be predicted, if a 3D multicable construction is carried out, the ship could lose power in the case of turbulence, the multiple cables could twist together, and the equipment could be destroyed, and there is a great risk in the operation. Therefore, multicable 3D seismic surveys are rarely carried out in this sea area.

2. Materials and Methods

2.1. Quasi-3D Seismic Data Acquisition

In special sea areas, we aim to achieve a balance between protecting the survey equipment and saving costs and acquiring data. The repeated two-dimensional observation system of “single-source single-cable high-density line spacing” is adopted. High-density 2D data are processed according to the 3D workflow, and thus, the 3D volume is obtained. In contrast to a true 3D seismic survey, it is called a “single-source and single-cable quasi-3D seismic survey” [9,13,14] (Figure 3). This method was first applied to the investigation of gas hydrate resources on the northern continental slope of the SCS [13–15].

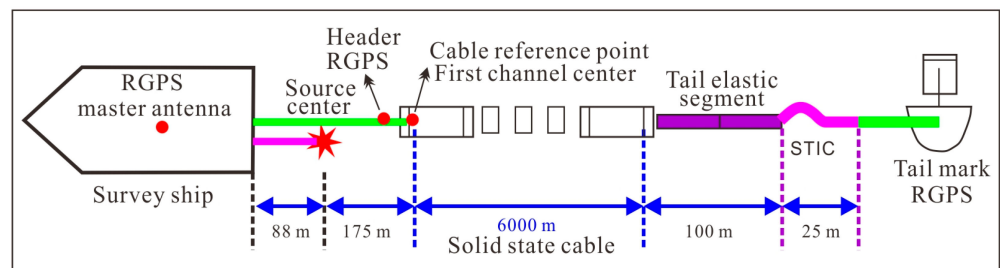


Figure 3. Relative position of the seismic source and cable.

A quasi-3D survey area of approximately 600 km² is formed in the Dongsha Waters in the northern SCS (Figure 1b). The acquisition parameters of quasi-3D seismic data are shown in Table 1.

Table 1. Seismic acquisition parameters.

Parameters	Value
Number of receiving trace	480
Distance between trace/m	12.5
Distance between shots/m	25
Coverage times	120
Sampling rate/ms	2
Source capacity/cu.in.	5080
Cable sinking depth/m	9
Minimum offset/m	225
Original bin size/m	25 × 100
The bin overlap rate	50%
Record length/s	8

The source design, cable source location and bin optimization are important to the acquisition of seismic data.

Firstly, the broadband source of the convex stereo delay array scheme (Figure 4) is designed to place the wavelet propagate deeply in the stratum, which is conducive to the deep imaging of the target layer [16]. It is composed of four equally spaced subarrays with sink depths of 8–5–5–8 m and excitation delay values of 2–0–0–2 ms.

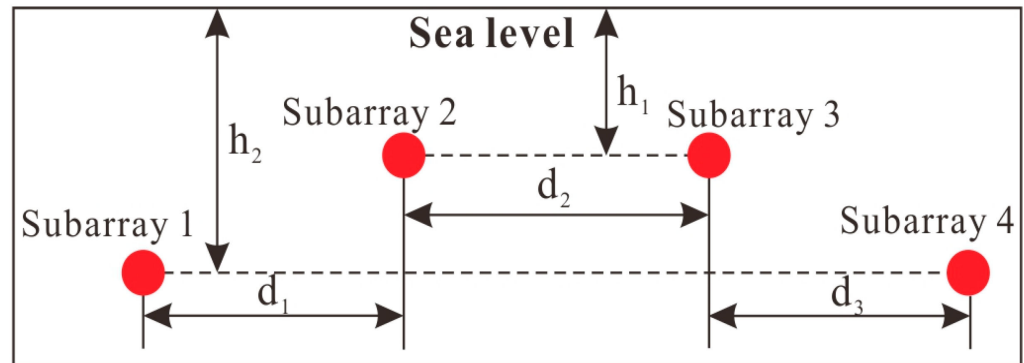


Figure 4. Schematic diagram of the stereoscopic source arrangement, in which $h_1 = 5$ m; $h_2 = 8$ m; $d_1 = d_2 = d_3$.

Secondly, for the quasi-3D seismic surveys, the imaging effect largely depends on the navigation and positioning accuracy [13,14]. According to the basic principle of the network positioning method [13], the “three-node network positioning method” technology is formed [17]. The three nodes are the source center node, the cable header node and the cable tail node. Each node is mainly used to determine the location reference point. An RGPS device is used to realize the positioning of the cable geophones between the reference points combined with the compass bird azimuth data from the cable. During construction, the towing cable is controlled and monitored according to the ship speed, tension, depth of sinking, the distribution of compass birds and transverse rudder birds and the drag of head and tail marks.

Thirdly, it is necessary to monitor the bin coverage, including real-time and processed data monitoring, to achieve 3D coverage. The operation sequence of the survey line is determined according to the law of tidal change. At the same time, the transverse rudder bird, which is controlled in real time, is used to modify the near, middle and far traces of the long cable, and the coverage of the bin is guaranteed through navigation and positioning control optimization in the acquisition process.

2.2. Data Processing

The OMEGA and GEOVATION systems are used for the joint processing of the seismic data. The main processing flow is shown in Figure 5. A variety of noises are suppressed according to the 2D survey line. The multiples are removed, and ghost waves are suppressed after defining the 3D geometry. The gathers are sorted by bin, and then, bin regularization and 3D prestack migration image processing are carried out. Bubble elimination, broadening frequency band (ghost wave suppression) and 3D bin regularization are the key technologies of quasi-3D processing [10,11], which are described in the next section.

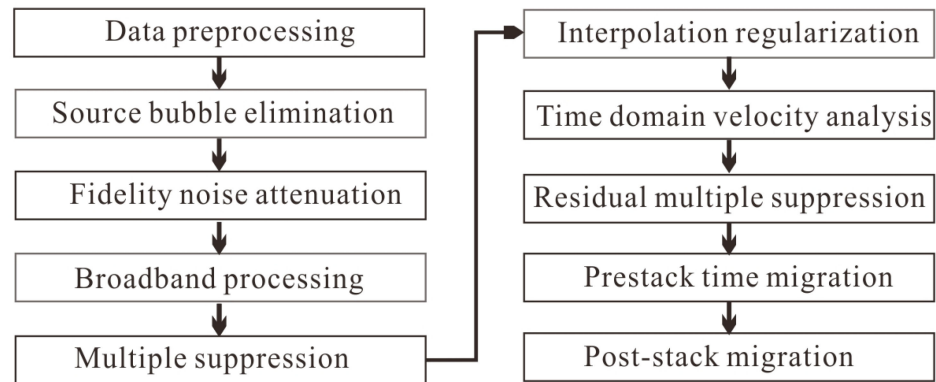


Figure 5. Quasi-3D seismic data processing flow.

3. Results

3.1. Seismic Fine Imaging

3.1.1. Source Bubble Elimination

Air-gun source excitation usually produces a long-period signal, which is accompanied by many side lobes whose amplitude decays over time. However, the main lobe is closely related to the underground geological structure. This series of side lobes is regarded as a bubble effect on the seismic profile [18]. After the bubble effect is suppressed, the “tail” of the source wavelet is eliminated (Figure 6). It can be seen that the resolution is improved and the energy is more focused after bubble removal. The attenuation of the bubble effect can be seen through direct wave comparison (red circles in Figure 6).

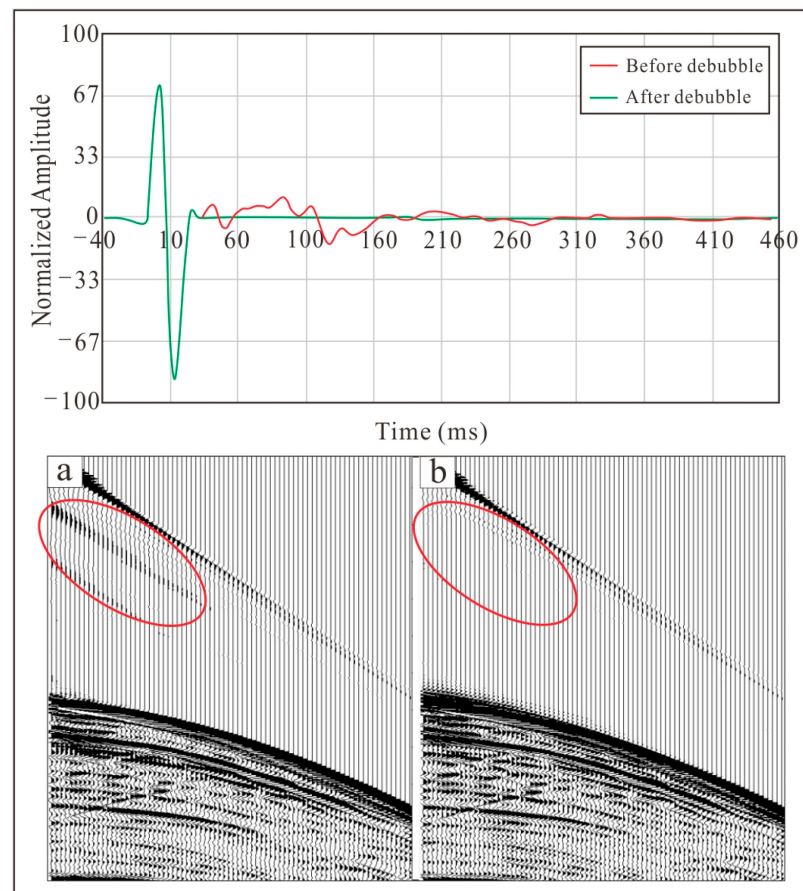


Figure 6. Wavelet (upper half) and gathers (lower half) comparison before (a) and after (b) the debubble.

3.1.2. Frequency Extension Processing (Deghost)

During the offshore seismic data acquisition, the source and geophone are placed below sea level, and sea level is regarded as a strongly reflective free surface. When the source seismic wave or formation reflected wave propagates to sea level, it will be reflected and propagated downward, which is called a ghost wave. The ghost wave is very similar to the primary wave. It reduces the resolution and forms a false event. A ghost wave will periodically lead to zero points in the seismic spectrum, which are called notch points. The notch phenomenon makes the frequency band of the seismic data narrower and the energy of the low-frequency band lower. Broadening the frequency band can improve the resolution and imaging effect of the seismic data. With the development of seismic data acquisition technology, a variety of broadband acquisition and processing methods have been proposed [19–22]. At present, conventional horizontal streamers are still the preferred method for offshore oil and gas exploration [23–25].

The sparse domain inversion of ghost wave removal technology is used to accurately estimate the delay time difference between the ghost waves and primary waves for ghost waves with different angles and spatial responses, restore the real seismic wavelets, compensate for the depression of the frequency band and broaden the frequency band. After the comparison was conducted, it can be seen that the imaging effect after broadband processing is richer in both the low frequencies and high frequencies (Figure 7). The interference of ghost waves is effectively suppressed, and the sidelobe of the wavelet is reduced, therefore, the data resolution of the geological structure and the reliability of interpretation are greatly improved (Figure 7).

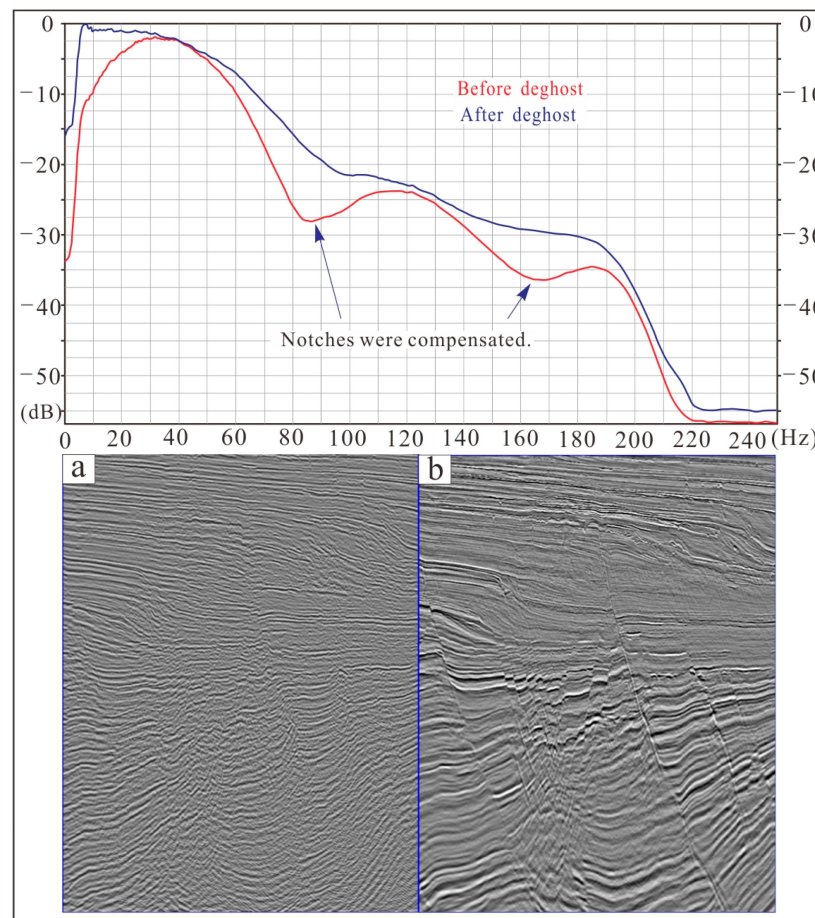


Figure 7. Spectral analysis and gathers before (a) and after (b) ghost wave removal.

3.1.3. 3D Bin Regularization (Interpolation)

The purpose of bin regularization processing is to make 2D acquisition data adapt to the requirements of 3D data processing through vertical and horizontal interpolation. Conventional interpolation techniques usually consider only three or four fields: the shot-point direction, the geophone point direction (or the inline and crossline directions, respectively), time and offset. Five-dimensional interpolation introduces azimuth information, which more closely follows the variation in the seismic data in time, space (X and Y), offset and azimuth. The comparison of the stacked profiles and time slices before and after five-dimensional interpolation (Figure 8) shows that it effectively compensates for the loss of the original data, removes the acquisition footprint and improves the signal-to-noise ratio of the data.

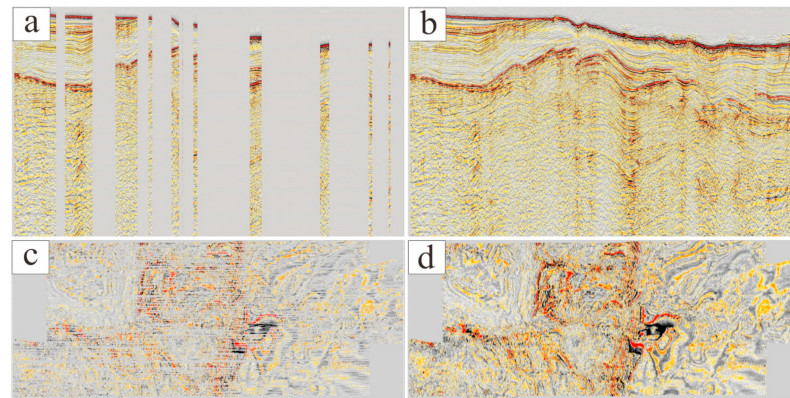


Figure 8. Comparison before and after five-dimensional interpolation ((a). profile before interpolation; (b). profile after interpolation; (c). time slice before interpolation; (d). time slice after interpolation).

From the imaging comparison between the 2D section and the quasi-3D section (extracted from the quasi-3D volume according to the 2D section coordinates), it can be seen that the imaging quality of the quasi-3D prestack time migration data is significantly better than that of the 2D section (Figure 9), especially in the middle and deep target layers, and the stratum reflection, fault breakpoints and structural morphology are clear.

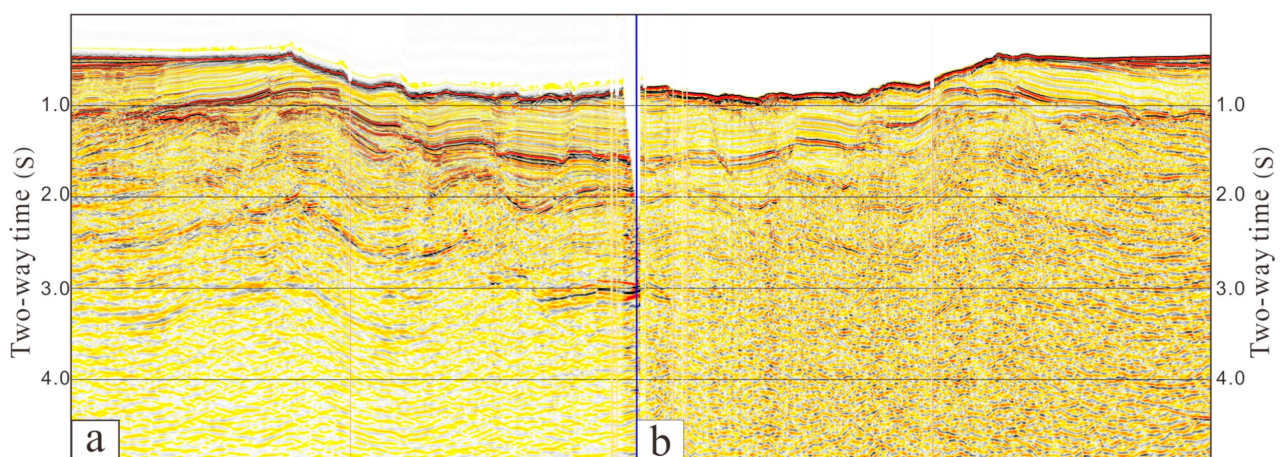


Figure 9. Effect comparison of the prestack time migration profile ((a). quasi-3D PSTM; (b). 2D PSTM).

3.2. Structural Reservoir Forming Model

In the turbulent sea area, the ideal migration imaging data volume is obtained by using the acquisition and processing techniques mentioned in this paper. On the quasi-3D profile, random and linear interferences and different types of multiple interferences are suppressed, and the effective information about the shallow, medium and deep layers is

highlighted. The sharpness and resolution of the reflection event imaging are improved. The diffracted wave converges and returns. The breakpoints, planes and boundaries of faults are clear.

Based on the quasi-3D data, six main interfaces (T_{j0} , T_{j1} , T_{j2} , T_{k0} , T_{k1} and T_g) are identified in the B-1 structure (see Figure 1 for the locations) of the Chaoshan depression (Figures 10 and 11). Together, they help us to define the structural reservoir-forming model (Figure 10) and define the local petroleum system [26–29]. Combined with previous research results [3,9], three sets of argillaceous source rocks in the Jurassic strata have developed. The reservoirs are mainly shallow sea sand bars at the top of the Lower Jurassic strata and the bottom of the Middle Jurassic strata, platform limestone at the top of the Middle Jurassic strata and slope fan sandstone at the middle and upper parts of the Upper Jurassic strata. The B-1 structure is located in the middle bump between the western sag and the eastern sag, and it is closer to the eastern sag. It is the “uplift in the middle of the depression” structure that is conducive to reservoirs. The oil and gas generated in the sags on both of the sides can be used as a dual-source hydrocarbon supply. As the structure is close to the hydrocarbon-generating sag, oil and gas accumulate in the high part of the structure through short-distance migration. The source rocks in the lower part of the middle-low uplift can also directly supply hydrocarbons upwards through the faults (Figure 10).

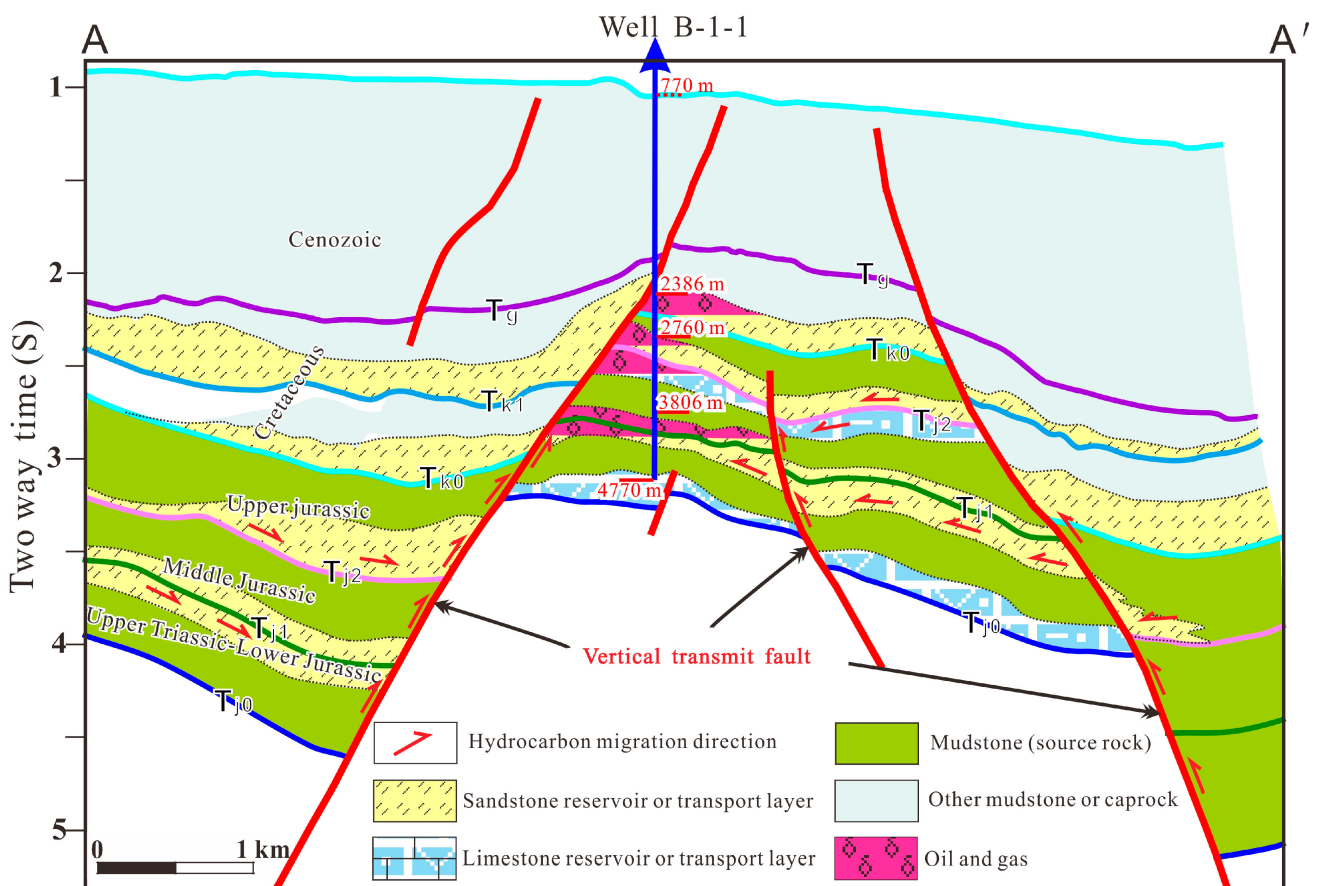


Figure 10. Prediction of the B-1 structural reservoir-forming model displaying elements of the local petroleum system.

3.3. Prediction of the Hydrate Development Area

In the southernmost part of the eastern sag (Figure 1b, B-B’), large spanning and visible BSRs [30–32] (Figure 12) are found, and highly organic carbon can be seen from the results of the geochemical survey [33]. The Mesozoic sequence is well developed, with the

T3-J1 and J3 hydrocarbon source rocks entering the mature–overmature period [33]. Faults F1, F2 and F3 cut deep into the Mesozoic strata and branch upward as F4, F5 and more fractures connect with them (Figure 10), forming a well passageway for the thermogenic gas to migrate upward to the Cenozoic strata (Figure 12). In addition, abundant authigenic carbonate nodules and deep water fauna, e.g., shells, corals and sponges, were found in the dredged samples above some mud volcanoes in the region, which implies the vigorous leakage of hydrocarbons [34]. Considering the gas leakage and the appearance of BSRs, the junction area between the middle bump and the southernmost part of the eastern sag deserves our attention.

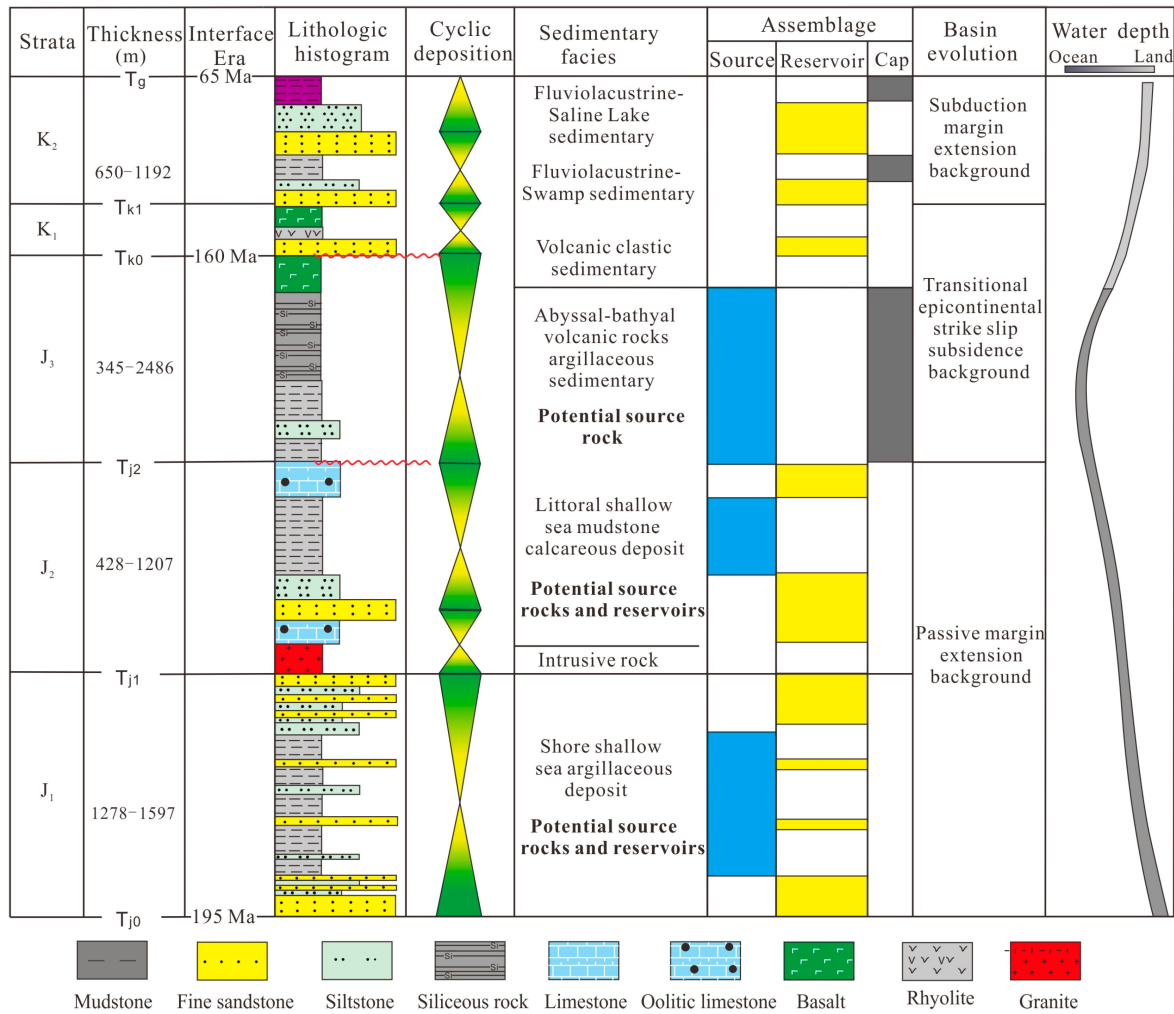


Figure 11. Comprehensive histogram of Chaoshan depression [3,26].

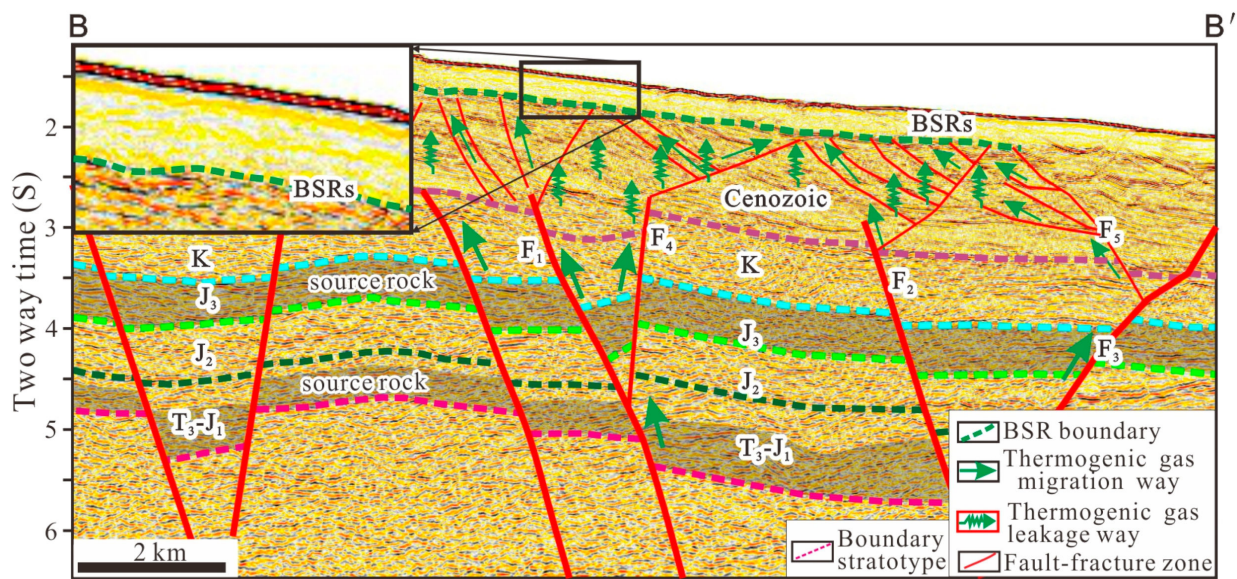


Figure 12. Hydrate accumulation pattern of section B-B'.

4. Discussion

The removal of the bubble effect transforms a narrowband, chirping signal into a broadband, compressed wavelet. The debubbling process does not depend on seismic reflection information [10,11]. In the first step of processing, it can better coordinate with the subsequent ghost wave removal process and avoid the “accidental damage” of the effective wave phenomenon in multiple wave adaptive subduction as much as possible. In the time domain, it is difficult to remove ghost waves because the delay time of ghost waves is a function of incident angle and time, and the time delay is not periodic. However, in the domain, the ray parameter is constant, and the delay time between the primary wave and the ghost wave is periodic, so it is much easier to eliminate the ghost wave [35]. The corresponding broadband inversion technology can provide more accurate information for oil and gas exploration. Five-dimensional interpolation can retain the original data trace, rather than simply replace it with an interpolation trace, to verify the fidelity of the interpolation. It should be pointed out that the quasi-3D collection method has its disadvantages, such as the imaging artifact caused by an overly narrow azimuth angle and an overly large CDP coverage ratio between the in-line and across-line directions.

Well LF35-1-1 was drilled in the northern slope of the Chaoshan depression in 2003 (Figure 1b). The results confirmed the existence of the Mesozoic strata in the northern SCS and revealed that the depositional environment of this area experienced a complete sedimentary and tectonic cycle from the Early Jurassic to the Early Cretaceous periods, including basin expansion and subsidence, deep water deposition, volcanic eruption and continental return [36,37] (Figure 11). The depression is filled with Cretaceous continental deposits and mid-late Jurassic marine deposits [38,39]. Although no hydrocarbons were found, the well encountered radiolarian-rich marine Mesozoic strata and Jurassic rocks with a high organic matter abundance, which confirm the existence of the Mesozoic marine residual basin. The existence of organic-rich rocks may be possible source rocks in the Chaoshan depression.

Based on the quasi-3D seismic data interpretation, we focused on the B1 structure in the middle bump of the Chaoshan depression. The B1 structure is located to the east of the middle bump, close to the eastern sag, and it contains rich argillaceous source rocks that are in the mature-overmature stage. According to the results of the geophysical prediction, the target layer in the Jurassic strata of this structure is sandstone. The mudstone caprock overlying the target layer is stable. A good reservoir-cap assemblage is conducive to hydrocarbon accumulation and preservation. The peak period of hydrocarbon generation

and expulsion is accurately matched with the time of the trap formation. Based on the above information, an exploratory well, B-1-1, is arranged in the B1 structure (Figure 10).

Geochemical anomaly areas are correlated with the Mesozoic fault distribution. Geochemical anomalies above the fault zones are usually common. Many faults cut through two sets of source rocks from Mesozoic strata to Cenozoic strata. The Cenozoic strata in this area are relatively thin, generally less than 1000 m. We are more inclined to think that thermogenic gas mainly comes from the Mesozoic strata [33].

5. Conclusions

The long-array and large-capacity quasi-3D seismic exploration method involves the 2D high-density acquisition of data by shooting a signal from a single composite source and receiving it using a single long cable, on-site quality control according to the 3D bin coverage during field construction and the 3D method used for indoor seismic data processing to finally form a 3D volume. Many special technologies are used in data acquisition and processing. The signal-to-noise ratio and the resolution of the obtained seismic data were significantly improved. It is suitable for complex sea areas where turbulence develops and true 3D seismic acquisition cannot be carried out.

Combined with the existing drilling and interpretation of the new data, a key structure B-1 is selected in the study area for the oil and gas accumulation model analysis. Structure B-1 has optimal reservoir-forming conditions. The exploration well, B-1-1, has been proposed in this structure, which is expected to further clarify the Mesozoic stratigraphic characteristics in the northern SCS and make a breakthrough in oil and gas exploration.

The source of thermogenic gas in the Chaoshan depression is sufficient [33]. Faults play a key role in hydrate accumulation in this area. The deep fault connects the stability zone of the hydrate and the inferred Mesozoic source rock. We suggest that deep thermogenic gas migrates along the fracture system to the overlying strata, mixes with microbial gas, and finally forms hydrate.

Author Contributions: Conceptualization and methodology, Z.Z. and G.Z.; formal analysis, Z.Z., C.F., G.T. and H.Y.; original draft preparation, Z.Z. and M.S. All authors have read and agreed to the published version of the manuscript.

Funding: This research was funded by the China Geological Survey (Project No: DD20190212, DD20221860) and the National Natural Science Foundation of China (Grant No. 42076218).

Institutional Review Board Statement: Not applicable.

Informed Consent Statement: Not applicable.

Data Availability Statement: Data are available on request from the author Z.Z. (zzqhello@163.com).

Acknowledgments: We are grateful to all colleagues who participated in seismic acquisition and processing. Thank Zhang Jiajia and Ren Jiangbo for improving the manuscript.

Conflicts of Interest: The authors declare no conflict of interest.

References

1. Klemme, H.D.; Ulmishek, G.F. Effective petroleum source rocks of the world: Stratigraphic distribution and controlling depositional factors. *Am. Assoc. Pet. Geol. Bull.* **1991**, *75*, 1809–1851.
2. Qiang, K.; Zhang, G.; Zhang, G.; Zhang, L.; LV, B.; Zhong, G.; Feng, C.; YI, H.; Zhao, Z.; Yang, Z.; et al. A study of depositional characteristics of the Jurassic strata in Chaoshan Subbasin, northern South China Sea, and its control on reservoir bed. *Geol. China* **2018**, *45*, 48–58.
3. Zhao, Z.; Sun, M.; Wan, X.; Chen, S.; Zhao, J.; Song, L.; Li, H.; Qiang, K.; Liang, Y. The application of microbial exploration technology to the oil and gas survey of Chaoshan depression. *Geol. China* **2020**, *47*, 645–654.
4. Zhou, D.; Wang, W.; Wang, J. Mesozoic subduction-accretion zone in northeastern South China Sea inferred from geophysical interpretations. *Sci. China Ser. D* **2006**, *49*, 471–482. [[CrossRef](#)]
5. Udo, B.; Martin, E.; Dieter, F.; Stefan, L.; Manuel, P. Evolution of the South China Sea: Revised ages for breakup and seafloor spreading. *Mar. Pet. Geol.* **2014**, *58*, 599–611.

6. Chen, B.; Wang, J.; Zhong, H.; Chen, H.; Hao, H.; Li, P. A study on fault distribution and tectonic framework in Northeastern South China Sea. *J. Trop. Oceanogr.* **2005**, *2*, 42–51.
7. Hu, W.; Jiang, W.; Hao, T.; Xu, Y.; Zhao, B. Integrated geophysical research on the distribution of Pre-Cenozoic residual basins in the South China Sea. *Chin. J. Geophys.* **2011**, *54*, 3315–3324. [[CrossRef](#)]
8. Zhang, G.; Qu, H.; Liu, S.; Xie, X.; Zhao, Z.; Shen, H. Hydrocarbon accumulation in the deep waters of South China Sea controlled by the tectonic cycles of marginal sea basins. *Pet. Res.* **2016**, *1*, 39–52. [[CrossRef](#)]
9. Xing, T.; Zhong, G.; Zhan, W.; Zhao, Z.; Chen, X. Oil-gas reservoir in the Mesozoic strata in the Chaoshan depression, northern South China Sea: A new insight from long offset seismic data. *J. Oceanol. Limnol.* **2022**, *40*, 1377–1387. [[CrossRef](#)]
10. Deng, G.; Ding, L.; Li, F.; Zhang, B. The processing technology of narrow azimuth Quasi three-dimensional seismic data acquisition by single source and single long streamer system in marine seismic exploration. *Geophys. Geochem. Explor.* **2019**, *43*, 828–834.
11. Xing, T.; Chen, H.; Zhang, B. High-density bispectral velocity analysis on gas hydrates seismic data processing in Chinese maritime Xisha, South China Sea. *Oceanol. Limnol. Sin.* **2015**, *46*, 272–277.
12. Wei, C.; Hao, X.; Yi, H.; Wu, Z.; Yang, S.; Gu, C. Design and application of seismic exploration source for the Mesozoic group in the northern South China Sea. *Oil Geophys. Prospect.* **2012**, *47*, 1–7+162.
13. Andreas, C. Narrow versus wide-azimuth land 3D seismic surveys. *Lead. Edge* **2002**, *21*, 764–770.
14. Davidson, D.W.; Ripeester, J.A. *Water: A Comprehensive Treatise*; Plenum Press: New York, NY, USA, 2006; pp. 21–33.
15. Zhao, Q. Optimized bin parameter on gas-hydrate quasi-three-dimensional seismic survey. *J. Trop. Oceanogr.* **2011**, *1*, 70–77.
16. Wei, C.; Yang, S.; Guan, X.; Zhang, R.; Zeng, X.; Hao, X. A delayed updown subarray airgun source. *Oil Geophys. Prospect.* **2014**, *49*, 1027–1033.
17. Zhang, M.; Peng, Z.; Sha, Z. The navigation and positioning technique for pseudo 3D seismic survey in natural gas hydrate exploration. *Mar. Geol. Quat. Geol.* **2008**, *6*, 101–106.
18. Can, O.; Robert, L.N. An overview of reproducible 3D seismic data processing and imaging using Madagascar. *Geophysics* **2018**, *83*, F9–F20.
19. Nick, M.; Leendert, C.; Mark, E.; Gary, H.; Larry, S.; William, A. Over/under towed-streamer acquisition: A method to extend seismic bandwidth to both higher and lower frequencies. *Lead. Edge* **2007**, *26*, 41–58.
20. Hill, D.; Combee, C.; Bacon, J. Over/under acquisition and data processing: The next quantum leap in seismic technology? *First Break* **2006**, *24*, 81–95. [[CrossRef](#)]
21. Kroode, F.; Bergler, S.; Corsten, C.; Willem, J.; Strijbos, F.; Tijhof, H. Broadband seismic data—the importance of low frequencies. *Geophysics* **2013**, *78*, WA3–WA14. [[CrossRef](#)]
22. Guan, X.; Chen, B.; Fu, L.; Tao, J.; Li, L. The study of a deghosting method of over/under streamer seismic data based on wave equation. *Chin. J. Geophys.* **2015**, *10*, 3746–3757.
23. Adriana, C.R.; Weglein, A.B. Green’s theorem as a comprehensive framework for data reconstruction, regularization, wavefield separation, seismic interferometry, and wavelet estimation: A tutorial. *Geophysics* **2009**, *74*, W35–W62.
24. James, D.M.; Weglein, A.B. First application of Green’s theorem derived source and receiver deghosting on deep water Gulf of Mexico synthetic (SEAM) and field data. *Geophysics* **2013**, *78*, WA77–WA89.
25. Xie, Y.; Hu, T. Marine seismic data deghosting with 1.5D inverse scattering series method. *Acta Sci. Nat. Univ. Pekin.* **2018**, *54*, 535–545.
26. Magoon, L.B.; Dow, W.G. (Eds.) *The Petroleum System—From Source to Trap*; American Association of Petroleum Geologists: Tulsa, OK, USA, 1994; pp. 3–24.
27. Burton, Z.F.M.; Moldowan, J.M.; Magoon, L.B.; Sykes, R.; Graham, S.A. Unraveling petroleum degradation, maturity, and mixing and addressing impact on petroleum prospectivity: Insights from frontier exploration regions in New Zealand. *Energy Fuels* **2018**, *32*, 1287–1296. [[CrossRef](#)]
28. Burton, Z.F.M.; Moldowan, J.M.; Magoon, L.B.; Sykes, R.; Graham, S.A. Interpretation of source rock depositional environment and age from seep oil, east coast of New Zealand. *Int. J. Earth Sci.* **2019**, *108*, 1079–1091. [[CrossRef](#)]
29. Thompson-Butler, W.; Peters, K.E.; Magoon, L.B.; Scheirer, A.H.; Moldowan, J.M.; Blanco, V.O.; Gonzalez, R.E.; Graham, S.A.; Zumberge, J.E.; Wavrek, D.A. Identification of genetically distinct petroleum tribes in the Middle Magdalena Valley, Colombia. *AAPG Bull.* **2019**, *103*, 3003–3034. [[CrossRef](#)]
30. Shipley, T.H.; Houston, M.H.; Buffler, R.T.; Shaub, F.J.; Mcmillen, K.J.; Laod, J.W.; Worzel, J.L. Seismic evidence for widespread possible gas hydrate horizons on continental slopes and rises. *AAPG Bull.* **1979**, *63*, 2204–2213.
31. Hyndman, R.D.; Spence, G.D. A seismic study of methane hydrate marine bottom simulating reflectors. *J. Geophys. Res. Solid Earth* **1992**, *97*, 6683–6698. [[CrossRef](#)]
32. Burton, Z.F.M.; Kroeger, K.F.; Hosford Scheirer, A.; Seol, Y.; Burgreen-Chan, B.; Graham, S.A. Tectonic uplift destabilizes subsea gas hydrate: A model example from Hikurangi margin, New Zealand. *Geophys. Res. Lett.* **2020**, *47*, e2020GL087150. [[CrossRef](#)]
33. Feng, C.; Zhong, G.; Sun, M.; Lei, Z.; Yi, H.; Zhao, Z. Analysis of the thermogenic gas source of natural gas hydrates over the Dongsha Waters, in the northern South China Sea. *Front. Earth Sci.* **2022**, *10*, 873615. [[CrossRef](#)]
34. Yan, P.; Wang, Y.L.; Jin, Y.; Zhao, M.; Zhong, G. Deep-water coral of multiple benthic strategies discovered from mounds in the Dongsha Waters in the South China Sea. *Front. Earth Sci.* **2022**, *29*, 202–210.

35. Zhang, X.; Pan, D.; Shi, W.; Fang, Z.; Dan, Z.; Zhang, L. Deghosting towed streamer data in τ/p domain based on rough sea surface reflectivity. *Appl. Geophys.* **2015**, *4*, 573–584+629. [[CrossRef](#)]
36. Hao, H.; Shi, H.; Zhang, X.; Jiang, T.; Tang, S. Mesozoic sediments and their petroleum geology conditions in Chaoshan sag: A discussion based on drilling results from the exploratory well LF35-1-1. *China Offshore Oil Gas* **2009**, *21*, 151–156.
37. Shao, L.; You, H.; Hao, H.; Wu, G.; Qiao, P.; Lei, Y. Petrology and depositional environments of Mesozoic strata in the Northeastern South China Sea. *Geol. Rev.* **2007**, *02*, 164–169.
38. Wu, G.; Wang, R.; Hao, H.; Shao, L. Microfossil evidence for development of marine Mesozoic in the North of South China Sea. *Mar. Geol. Quat. Geol.* **2007**, *1*, 79–85.
39. Zhong, G.; Wu, S.; Feng, C. Sedimentary model of Mesozoic in the northern South China Sea. *J. Trop. Oceanogr.* **2011**, *30*, 43–48.

Disclaimer/Publisher’s Note: The statements, opinions and data contained in all publications are solely those of the individual author(s) and contributor(s) and not of MDPI and/or the editor(s). MDPI and/or the editor(s) disclaim responsibility for any injury to people or property resulting from any ideas, methods, instructions or products referred to in the content.